ISSN 1063-7788, Physics of Atomic Nuclei, 2014, Vol. 77, No. 11, pp. 1378–1389. © Pleiades Publishing, Ltd., 2014.
Original Russian Text © V.I. Kuprikov, V.V. Pilipenko, 2014, published in Yadernaya Fizika, 2014, Vol. 77, No. 11, pp. 1443–1554.

NUCLEI
Theory

Elastic Proton–Nucleus Scattering in the Glauber–Sitenko Approach and Relativistic and Nonrelativistic Nuclear Mean Fields

V. I. Kuprikov* and **V. V. Pilipenko****

National Science Center, Kharkiv Institute of Physics and Technology, Akademicheskaya ul. 1, 61108 Kharkiv, Ukraine

Received January 9, 2014

Abstract—The differential cross sections for elastic proton scattering on ^{40}Ca and ^{208}Pb nuclei at 800 MeV are analyzed along with respective spin observables on the basis of the Glauber–Sitenko approach with allowance for two-nucleon correlations, these correlations being taken into account via the inclusion of intermediate excitations of target nuclei and noneikonal corrections. The possibility of employing, in these calculations, realistic nucleon densities obtained in describing the structure of nuclei on the basis of the relativistic- and nonrelativistic-mean-field approximations with various versions of nucleon-interaction parameters is explored. It is shown that some of the nucleon-density versions considered here provide a reasonable description of experimental data, allowance for intermediate nuclear excitations and noneikonal corrections being substantial for ensuring agreement with these data.

DOI: 10.1134/S106377881410010X

1. Glauber–Sitenko theory of multiple diffractive scattering [1–3] is quite a successful approach to analyzing processes of intermediate-energy hadron–nucleus and nucleus–nucleus scattering. In recent years, the model of relativistic impulse approximation (RIA) has also been used to study proton–nucleus scattering (see, for example, [4, 5] and references therein). The RIA model is based on solving the Dirac equation with a relativistic microscopic optical potential. Nevertheless, the theory of multiple diffractive scattering is still widely used to analyze various processes induced by the scattering of nucleons and nuclei (see, for example, [6, 7] and references therein).

Differential cross sections and spin observables have been measured precisely for proton–nucleus scattering at intermediate energies of about several hundred MeV units, and respective data can be found in the literature. From an analysis of these data, one can hope to derive valuable information about the structure of nuclei—in particular, about nucleon densities and about distinctions between the distributions of protons and neutrons in nuclei, as well as about nucleon correlations. However, accurate theoretical methods are required for reliably analyzing such data. In describing proton scattering at intermediate energies, the theory of multiple diffractive scattering is a good first approximation. In order to perform a more accurate quantitative analysis of the data, it is necessary to refine upon this approach. In our previous studies [8, 9], expressions that were free from a number of frequently used simplifications and which take into account, in the calculations, two-nucleon correlations via the inclusion of intermediate excitations of target nuclei were obtained for proton–nucleus amplitudes within the theory in question. The calculations performed on the basis of this approach and reported in [8, 9] made it possible to describe reasonably the data and showed the need for taking into account the corrections in question.

In the present study, this approach is used to perform a comparative analysis of the application of realistic nucleon densities found from independent calculations of the nuclear structure on the basis of the relativistic- and nonrelativistic-mean-field approximations with various versions of nucleon-interaction parameters in describing cross sections for elastic proton–nucleus scattering and respective polarization observable. Since the theory in question is the theory of multiple eikonal scattering on intranuclear nucleons, it would be reasonable in performing calculations to consider the effect of taking into account noneikonal corrections to the scattering amplitude. For this reason, we extend here the model in such a way as to include the corrections in question and study the effect of taking them into account, along with nucleon correlations, on the description of observables of the scattering process. On the basis of this approach, we thereupon perform the aforemen-

*E-mail: vkuprikov@kipt.kharkov.ua
**E-mail: vpilipenko@kipt.kharkov.ua

tioned comparative analysis for the elastic scattering of 800-MeV protons on ^{40}Ca and ^{208}Pb nuclei.

2. The expressions that we use for the proton–nucleus amplitudes take into account the distinctions between the proton–proton and proton–neutron amplitudes and between the densities of neutrons and protons, Z ordering of spin operators, and electromagnetic effects; also, they are free from a number of simplifications and are similar to those presented in [8, 9]. For the operator of the amplitude for elastic proton–nucleus scattering, the theory of multiple diffractive scattering yields

$$F_e(\mathbf{q}) = A(q) + B(q)\,\boldsymbol{\sigma}\mathbf{n} = \frac{ik}{2\pi}\int d^2b e^{i\mathbf{qb}}\Omega_e(\mathbf{b}), \quad (1)$$

where the profile function corresponding to elastic scattering has the form

$$\Omega_e(\mathbf{b}) = 1 - \left\langle 0\left|\hat{Z}\prod_{j=1}^{A} S_j(\mathbf{b}-\mathbf{r}_{j\perp})\right|0\right\rangle, \quad (2)$$

$$S_j(\mathbf{b}) = 1 - \frac{1}{2\pi ik}\int d^2q e^{-i\mathbf{qb}} f_j(\mathbf{q}).$$

Here, k is the wave vector; $\boldsymbol{\sigma}$ are the Pauli matrices; $\mathbf{n} = \mathbf{k}_i \times \mathbf{k}_f/|\mathbf{k}_i \times \mathbf{k}_f|$ ($\mathbf{k}_i$ and $\mathbf{k}_f$ are, respectively, the initial and the final wave vector); $\mathbf{q}$ and $\mathbf{b}$ are the momentum transfer and the impact parameter, respectively; $|0\rangle$ is the ground-state vector of the target nucleus; $\mathbf{r}_{j\perp}$ is the projection of the j-nucleon radius vector onto a plane orthogonal to the beam; A is the mass number of the target nucleus; and $\hat{Z}$ is the Z-ordering operator. In the cases of nuclei whose spin is zero, the spin–spin components of the nucleon–nucleon (NN) amplitude make but a small contribution [10] to the amplitude for proton–nucleus scattering, and one usually disregards them in such calculations on the basis of the theory of multiple diffractive scattering. For this reason, we take into account in the proton–nucleon (pN) amplitudes $f_j(\mathbf{q})$ only the central and spin–orbit terms ($j = p, n$); that is,

$$f_j(\mathbf{q}) = f_c^{(j)}(q) + f_s^{(j)}(q)\,\boldsymbol{\sigma}\mathbf{n}. \quad (3)$$

We represent the proton–nucleus profile function in the form [8, 9] $\Omega_e(\mathbf{b}) = \Omega_0(b) + \Omega^{(\mathrm{ex})}(\mathbf{b})$, where the term $\Omega_0(b)$ describes scattering without allowance for nucleon correlations ($\mathbf{B} = \mathbf{e}_b \times \mathbf{e}_z$, $Oz||\mathbf{k}$); that is,

$$\Omega_0(\mathbf{b}) = \Omega_{c0}(b) + i\boldsymbol{\sigma}\mathbf{B}\Omega_{B0}(b), \quad (4)$$

$$\Omega_{c0}(b) = 1 - C_{N,Z}^{(+)}(b),$$

$$\Omega_{B0}(b) = iC_{N,Z}^{(-)}(b),$$

$$C_{N,Z}^{(\pm)}(b) = \frac{1}{2}\left\{\left[1 - E_0^{(n)} + iE_s^{(n)}\right]^N \times \left[1 - E_0^{(p)} + iE_s^{(p)}\right]^Z \pm \left[1 - E_0^{(n)} - iE_s^{(n)}\right]^N \times \left[1 - E_0^{(p)} - iE_s^{(p)}\right]^Z\right\}, \quad (5)$$

$$E_{0,s}^{(j)}(b) = -\frac{i}{k}\int_0^\infty dqqJ_{0,1}(qb) f_{c,s}^{(j)}(q)\, Q_0^{(j)}(q), \quad (6)$$

where

$$Q_0^{(j)}(q) = 4\pi\int_0^\infty drr^2 j_0(qr)\rho_0^{(j)}(r)$$

are the nucleon ($j = p, n$) form factors for the ground state of the target nucleus (hereafter, $J_m(x)$ and $j_m(x)$ are, respectively, cylindrical and spherical Bessel functions). The term $\Omega^{(\mathrm{ex})}(\mathbf{b})$ takes into account two-nucleon correlations via the inclusion of the terms in the profile function that correspond to intermediate excitations of various multipolarity I for target nuclei and which have the form [8]

$$\langle 0|S_A|0\rangle \cdots \langle 0|S_i|\alpha; I, M\rangle \cdots \langle \alpha; I, M|S_j|0\rangle \cdots \langle 0|S_1|0\rangle,$$

where M is the projection of the spin $\mathbf{I}$ and α stands for the remaining quantum numbers of the state being considered. The operator $\Omega^{(\mathrm{ex})}(\mathbf{b})$ can be represented in the form

$$\Omega^{(\mathrm{ex})}(\mathbf{b}) = \Omega_{c1}^{(\mathrm{ex})}(b) + \Omega_{c2}^{(\mathrm{ex})}(b) + i\boldsymbol{\sigma}\mathbf{B}\left[\Omega_{B1}^{(\mathrm{ex})}(b) + \Omega_{B2}^{(\mathrm{ex})}(b)\right], \quad (7)$$

$$\Omega_{c1}^{(\mathrm{ex})}(b) = -\sum_{\alpha,I,M} Y_{IM}^2\left(\frac{\pi}{2}, 0\right) \times \sum_{\nu=0}^{2} k_\nu\left\{C_{N-\nu,Z-2+\nu}^{(+)}\left[E_{IM}^{(\alpha,i_\nu)}E_{IM}^{(\alpha,j_\nu)} - \left(\frac{d}{db}E_{sIM}^{(\alpha,i_\nu)}\right)\left(\frac{d}{db}E_{sIM}^{(\alpha,j_\nu)}\right)\right] + iC_{N-\nu,Z-2+\nu}^{(-)}\left[E_{IM}^{(\alpha,i_\nu)}\frac{d}{db}E_{sIM}^{(\alpha,j_\nu)} + E_{IM}^{(\alpha,j_\nu)}\frac{d}{db}E_{sIM}^{(\alpha,i_\nu)}\right]\right\}, \quad (8)$$

$$\Omega_{B1}^{(\mathrm{ex})}(b) = \sum_{\alpha,I,M} Y_{IM}^2\left(\frac{\pi}{2}, 0\right) \times \sum_{\nu=0}^{2} k_\nu\left\{iC_{N-\nu,Z-2+\nu}^{(-)}\left[E_{IM}^{(\alpha,i_\nu)}E_{IM}^{(\alpha,j_\nu)}\right.\right. \quad (9)$$

$$- \left(\frac{d}{db}E_{sIM}^{(\alpha,i_\nu)}\right)\left(\frac{d}{db}E_{sIM}^{(\alpha,j_\nu)}\right)\Bigg]$$
$$- C_{N-\nu,Z-2+\nu}^{(+)}\Bigg[E_{IM}^{(\alpha,i_\nu)}\frac{d}{db}E_{sIM}^{(\alpha,j_\nu)}$$
$$+ E_{IM}^{(\alpha,i_\nu)}\frac{d}{db}E_{sIM}^{(\alpha,j_\nu)}\Bigg]\Bigg\},$$

$$\Omega_{c2}^{(\mathrm{ex})}(b) \approx \sum_{\alpha,I,M} Y_{IM}^2\left(\frac{\pi}{2},0\right)\frac{M^2}{b^2} \qquad (10)$$
$$\times \sum_{\nu=0}^{2} k_\nu E_{sIM}^{(\alpha,i_\nu)} E_{sIM}^{(\alpha,j_\nu)} C_{N-\nu,Z-2+\nu}^{(+)},$$

$$\Omega_{B2}^{(\mathrm{ex})}(b) \approx -i\sum_{\alpha,I,M} Y_{IM}^2\left(\frac{\pi}{2},0\right)\frac{M^2}{b^2} \qquad (11)$$
$$\times \sum_{\nu=0}^{2} k_\nu E_{sIM}^{(\alpha,i_\nu)} E_{sIM}^{(\alpha,j_\nu)} C_{N-\nu,Z-2+\nu}^{(-)},$$

$$E_{IM}^{(\alpha,j)}(b) = -\frac{i}{k}\int_0^\infty dqqJ_M(qb) f_c^{(j)}(q)\, Q_{\alpha I}^{(j)}(q)\,, \quad (12)$$

$$E_{sIM}^{(\alpha,j)}(b) = -\frac{i}{k}\int_0^\infty dqJ_M(qb) f_s^{(j)}(q)\, Q_{\alpha I}^{(j)}(q)\,.$$

The transition nucleon form factors are

$$Q_{\alpha I}^{(j)}(q) = 4\pi\int_0^\infty drr^2 j_I(qr)\rho_{\alpha I}^{(j)}(r),$$

and the indices i_ν and j_ν assume the values of $i_2 = i_1 = j_2 = n$ and $i_0 = j_1 = j_0 = p$. We also use the following notation: $k_0 = Z(Z-1)/2$, $k_1 = NZ$, and $k_2 = N(N-1)/2$.

We take into account two-nucleon correlations, including a number of the most important intermediate excitations. Correlations associated with the center-of-mass motion of the target nucleus are taken into account as the $I = 1$ intermediate excitation whose transition density has the form $\rho_{\mathrm{c.m.}}^{(j)}(r) = i\left[4\pi\Big/\left(Nr_m^{(n)2} + Zr_m^{(p)2}\right)\right]^{1/2} r\rho_0^{(j)}(r)$, where $r_m^{(n,p)}$ are the root-mean-square radii for the densities $\rho_0^{(n,p)}(r)$, this corresponding to taking into account center-of-mass motion as in [11]. We also take into account short-range correlations as transitions to continuum states, the transition density being $\tilde{\rho}_{\mathrm{sr}}^{(j)}(\mathbf{u},\mathbf{r}) = \rho_0^{(j)}(r)\left[\exp(-i\mathbf{ur}) - Q_0^{(j)}(u)\right]$. The respective sum over excited states has the form

$$\sum\nolimits_{\alpha,I,M,\ldots} \to (-1)/(2\pi)^3\int d^3u\zeta(u)\ldots,$$

where $\zeta(u) = 8l_{\mathrm{cor}}^3\exp\left(-u^2l_{\mathrm{cor}}^2/\pi\right)$, l_{cor} being the correlation length. The expressions for proton–nucleus amplitudes also take into account the electromagnetic interaction, including its spin–orbit part. In contrast to what one has within the macroscopic approach developed in [10], this part appears in the proton–nucleon amplitudes; that is, $f_c^{(j)}(q) = f_{cN}^{(j)}(q)$, $f_s^{(n)}(q) = f_{sN}^{(n)}(q)$, and $f_s^{(p)}(q) = f_{sN}^{(p)}(q) + f_{s,\mathrm{em}}^{(p)}(q)$, where $f_{cN}^{(j)}(q)$ and $f_{sN}^{(j)}(q)$ are nuclear amplitude components calculated by using nuclear phase shifts found from a partial-wave analysis. The electromagnetic spin–orbit correction $f_{s,\mathrm{em}}^{(p)}(q)$ is taken in the same form as in the partial-wave analysis reported in [12].

In the simplest version of this approach [8, 9], the transition densities for intermediate excitations can be expressed in terms of the nucleon densities within the macroscopic model, while the corresponding deformation lengths can be determined from the known values of $B(EI)$ [13, 14] or taken from the studies where these transitions were analyzed on the basis of a similar macroscopic model.

Some deviations of the calculated observables [8, 9] from experimental data indicate that a further refinement upon the approach based on the theory of multiple diffractive scattering is necessary for performing a more accurate quantitative analysis of cross sections and polarizations. This theory is the theory of eikonal multiple scattering of a projectile particle on target nucleons and disregards the transverse motion of this particle; therefore, it is necessary to assess the effect of taking into account noneikonal corrections to the scattering amplitude and to include simultaneously nucleon correlations. It should be noted that noneikonal corrections are compensated to a significant extent by other corrections to the theory of multiple diffractive scattering (for example, by corrections associated with the Fermi motion of nucleons in the target nucleus) [15]. Therefore, noneikonal corrections that can make a significant contribution are taken here into account within the approach developed in [16]. This approach relies on a number of assumptions that take into account the cancellation of some corrections to the theory of multiple diffractive scattering—namely, one can disregard the motion of nucleons within the target nucleus during the interaction with a projectile proton and the contribution of repeated particle scattering on the same nucleon. The most important matrix elements of the transition operator t_j for proton scattering on the jth intranuclear nucleon may then be assumed to be local on-shell quantities.

Expressions for taking into account noneikonal corrections to the theory of multiple diffractive scattering can be obtained from Watson's multiple-scattering series [17] for the transition operator in proton–nucleus scattering, T, upon truncating this series at the term of order A and upon taking into account only single scattering on each nucleon; that is,

$$T = \sum_{j=1}^{A} t_j + \sum_{j=1}^{A}\sum_{k\neq j}^{A} t_j G^{(+)} t_k + \sum_{j=1}^{A}\sum_{k\neq j}^{A}\sum_{l\neq k\neq j}^{A} t_j G^{(+)} t_k G^{(+)} t_l + \ldots + \text{terms of order } A. \quad (13)$$

Within the approach used, the sought corrections to the theory of multiple diffractive scattering stem from taking into account the first noneikonal terms in the expansion of the propagator $G^{(+)}$ for free proton motion between events of scattering on target nucleons in a power series in $1/k$: $G^{(+)} \approx G^{(+)}_{\text{eik}} + \delta G^{(+)}_{\text{ne}}$. The expressions for the eikonal propagator and first-order noneikonal correction then have the form [16]

$$G^{(+)}_{\text{eik}} = -\left[2\mathbf{k}_a\left(\hat{\mathbf{k}} - \mathbf{k}_a\right) - i0\right]^{-1}, \quad (14)$$

$$\delta G^{(+)}_{\text{ne}} = \frac{\left(\hat{\mathbf{k}} - \mathbf{k}_a\right)^2 - q^2/4}{\left[2\mathbf{k}_a\left(\hat{\mathbf{k}} - \mathbf{k}_a\right) - i0\right]^2},$$

where $\mathbf{k}_a = (\mathbf{k}_i + \mathbf{k}_f)/2$ and $\hat{\mathbf{k}} = -i\partial/\partial\mathbf{r}$ is the momentum operator. Allowance for only the eikonal propagator $G^{(+)}_{\text{eik}}$ in Eq. (13) leads to standard expressions for the proton–nucleus scattering amplitude in the eikonal approximation of the theory of multiple diffractive scattering, while the inclusion of the contributions of $\delta G^{(+)}_{\text{ne}}$ yields noneikonal corrections to the amplitude. Omitting the details of the calculations, we only present the resulting ultimate formulas.

After taking into account noneikonal corrections, the profile function develops an additional term; that is, $\Omega_e(\mathbf{b}) = \Omega_0(b) + \Omega^{(\text{ex})}(\mathbf{b}) + \Omega^{(\text{ne})}(\mathbf{b})$. This term can be represented in the form $\Omega^{(\text{ne})}(\mathbf{b}) = \Omega^{(\text{ne})}_c(b) + i\boldsymbol{\sigma}\mathbf{B}\Omega^{(\text{ne})}_B(b)$. The profile functions $\Omega^{(\text{ne})}_c(\mathbf{b})$ and $\Omega^{(\text{ne})}_B(\mathbf{b})$ are given by

$$\Omega^{(\text{ne})}_c(b) = -\frac{i}{k}\sum_{\nu=0}^{2} k_\nu \left\{ g_0^{(i_\nu,j_\nu)}(b)\, C^{(+)}_{N-\nu,Z-2+\nu} + i\, g_B^{(i_\nu,j_\nu)}(b)\, C^{(-)}_{N-\nu,Z-2+\nu}\right\}, \quad (15)$$

$$\Omega^{(\text{ne})}_B(b) = \frac{i}{k}\sum_{\nu=0}^{2} k_\nu \left\{ i g_0^{(i_\nu,j_\nu)}(b)\, C^{(-)}_{N-\nu,Z-2+\nu} - g_B^{(i_\nu,j_\nu)}(b)\, C^{(+)}_{N-\nu,Z-2+\nu}\right\}. \quad (16)$$

In expressions (15) and (16), we have introduced the following notation:

$$g_0^{(i,j)}(b) = \int_{-\infty}^{\infty} dz \left\{ \left(1 + b\frac{d}{db}\right)\left[\varepsilon_0^{(i)}(r)\,\varepsilon_0^{(j)}(r)\right] - \left[\frac{d}{db}\varepsilon_1^{(i)}(r)\right]\left[\frac{d}{db}\varepsilon_1^{(j)}(r)\right] - \left\{\frac{1}{b}\varepsilon_1^{(i)}(r)\frac{d}{db}\varepsilon_1^{(j)}(r) + \left[\left(1 + b\frac{d}{db}\right)\varepsilon_1^{(i)}(r)\right]\frac{d^2}{db^2}\varepsilon_1^{(j)}(r) + (i \leftrightarrow j)\right\}\right\}, \quad (17)$$

$$g_B^{(i,j)}(b) = \int_{-\infty}^{\infty} dz \left\{ \frac{d}{db}\left[\varepsilon_0^{(i)}(r)\,\varepsilon_1^{(j)}(r)\right] + b\frac{d}{db}\left[\varepsilon_0^{(i)}(r)\frac{d}{db}\varepsilon_1^{(j)}(r)\right] + (i \leftrightarrow j)\right\}, \quad (18)$$

$$\varepsilon_0^{(j)}(r) = -\frac{i}{\pi k}\int_0^{\infty} dq q^2 j_0(qr) f_c^{(j)}(q)\, Q_0^{(j)}(q), \quad (19)$$

$$\varepsilon_s^{(j)}(r) = \frac{d}{db}\varepsilon_1^{(j)}(r), \quad (20)$$

$$\varepsilon_1^{(j)}(r) = -\frac{i}{\pi k}\int_0^{\infty} dq q j_0(qr) f_s^{(j)}(q)\, Q_0^{(j)}(q).$$

With allowance for electromagnetic interaction, the central component $A(q)$ and the spin–orbit component $B(q)$ of the amplitude in (1) for elastic proton scattering on a spinless nucleus are expressed in terms of the proton–nucleus profile function $\Omega_e(\mathbf{b}) = \Omega_c(b) + i\sigma\mathbf{B}\,\Omega_B(b)$ as

$$A(q) = A_C(q) + ik\int_0^{\infty} dbbJ_0(qb) \times \left\{e^{i\chi_0(b)} + e^{i\chi_1(b)}\left[\Omega_c(b) - 1\right]\right\}, \quad (21)$$

$$B(q) = B_C(q) - ik\int_0^{\infty} dbbJ_1(qb) \times \left[e^{i\chi_0(b)}\chi_{0s}(b) + e^{i\chi_1(b)}\Omega_B(b)\right]. \quad (22)$$

where $\chi_0(b) = 2\xi \ln(kb)$ and $\chi_{0s}(b) = 2\xi\kappa/b$ are, respectively, the central and spin–orbit phase shifts for two pointlike charges (proton and target nucleus) in the eikonal approximation, while the respective central and spin–orbit components of the scattering amplitude, $A_C(q)$ and $B_C(q)$, are given by

$$A_C(q) = -\frac{2\xi k}{q^2}\frac{\Gamma(1+i\xi)}{\Gamma(1-i\xi)}\exp\left(-2i\xi\ln\frac{q}{2k}\right), \quad (23)$$
$$B_C(q) = -i\kappa q A_C(q),$$

where $\xi = Ze^2/\hbar V$ is the Coulomb parameter for proton–nucleus scattering and the parameter κ characterizes the phase shift $\chi_{0s}(b)$ and the amplitude $B_C(q)$. The value of the parameter κ is determined from the asymptotic behavior of the profile function $\Omega_B(b)$ for $b \to \infty$; that is,

$$\kappa = -\frac{1}{2\xi}\lim_{b\to\infty}[b\mathrm{Re}\Omega_B(b)]. \quad (24)$$

The eikonal Coulomb phase $\chi_1(b)$ for scattering on the spatial charge distribution has the form [18]

$$\chi_1(b) = \chi_0(b) + 8\pi\xi\int_b^\infty dr r^2\rho_0^{(p)}(r) \quad (25)$$
$$\times\left[\ln\left(\frac{1+\sqrt{1-b^2/r^2}}{b/r}\right) - \sqrt{1-b^2/r^2}\right].$$

We recall that we take into account the interaction of the proton magnetic moment with the Coulomb field of the target nucleus microscopically through the proton–nucleon amplitudes.

3. In order to calculate the above proton–nucleus scattering amplitudes within the Glauber–Sitenko theory of multiple diffractive scattering, it is necessary to know the nucleon-density distributions in target nuclei. In the present study, we employ the nucleon densities that we find from microscopic calculations based on the relativistic- and nonrelativistic-mean-field (RMF and NRMF, respectively) approximations for target nuclei. The RMF and NRMF models, known from the literature, ensure a fairly good description of the ground-state properties of finite nuclei.

The RMF models used in the present study are based on the Lagrangian density for nuclei in the form (see, for example, [19–25]):

$$\mathcal{L} = \sum_{j=n,p}\bar\Psi_j\Big\{i\gamma^\mu\partial_\mu - M + g_\sigma\sigma - g_\omega\gamma^\mu\omega_\mu \quad (26)$$
$$-\frac{g_\rho}{2}\gamma^\mu\boldsymbol{\rho}_\mu\cdot\boldsymbol{\tau} - \frac{e}{2}\gamma^\mu(1-\tau_3)A_\mu\Big\}\Psi_j$$
$$+\frac{1}{2}\partial^\mu\sigma\partial_\mu\sigma - \frac{1}{2}m_\sigma^2\sigma^2 - \frac{g_2}{3}\sigma^3 - \frac{g_3}{4}\sigma^4$$
$$-\frac{1}{4}\Omega^{\mu\nu}\Omega_{\mu\nu} + \frac{1}{2}m_\omega^2\omega_\mu\omega^\mu + \frac{g_4}{4}(g_\omega^2\omega_\mu\omega^\mu)^2$$
$$+g_\sigma g_\omega^2\sigma\omega_\mu\omega^\mu\left(g_{\sigma\omega} + \frac{\bar g_{\sigma\omega}}{2}g_\sigma\sigma\right) - \frac{1}{4}\mathbf{R}^{\mu\nu}\mathbf{R}_{\mu\nu}$$
$$+\frac{1}{2}m_\rho^2\boldsymbol{\rho}_\mu\cdot\boldsymbol{\rho}^\mu + \frac{\bar g_{\omega\rho}}{2}g_\omega^2 g_\rho^2\omega_\mu\omega^\mu\boldsymbol{\rho}_\mu\cdot\boldsymbol{\rho}^\mu$$
$$+g_\sigma g_\rho^2\sigma\boldsymbol{\rho}_\mu\cdot\boldsymbol{\rho}^\mu\left(g_{\sigma\rho} + \frac{\bar g_{\sigma\rho}}{2}g_\sigma\sigma\right) - \frac{1}{4}F^{\mu\nu}F_{\mu\nu},$$

where σ, ω^μ, and $\boldsymbol{\rho}^\mu$ are, respectively, the scalar, isoscalar–vector, and isovector–vector meson fields ($\mu = 0, 1, 2, 3$); A_μ is the photon field (e is the coupling constant for the electromagnetic interaction of nucleons); $\Psi_{n,p}$ are the nucleon fields; $\boldsymbol{\tau}$ are the isospin Pauli matrices ($\tau_3 = 1$ for the neutron, and $\tau_3 = -1$ for the proton); γ^μ are the Dirac matrices; g_σ, g_ω, and g_ρ are the meson–nucleon coupling constants; m_σ, m_ω, and m_ρ are the meson masses; M is the nucleon mass; $\Omega_{\mu\nu}$ and $\mathbf{R}_{\mu\nu}$ are the vector-meson-field tensors; and $F_{\mu\nu}$ is electromagnetic-field tensor. In addition to meson–nucleon interactions, the Lagrangian density includes nonlinear scalar (the respective coupling constants are g_2 and g_3) and vector (the coupling constant is g_4) self-interactions, as well as mixed (the coupling constants are $g_{\sigma\omega}$, $\bar g_{\sigma\omega}$, $g_{\sigma\rho}$, $\bar g_{\sigma\rho}$, and $\bar g_{\omega\rho}$) interactions of the meson fields. All coupling constants and some meson masses are adjustable parameters of the models. They were determined in the literature from a fit to the properties of finite nuclei and infinite nuclear matter.

Since the conditions of symmetry and stationarity are imposed in deriving the equations of RMF approximation, only the time components of the four-vector nucleon and electromagnetic currents and vector meson fields are involved in these equations. A set of coupled equations that includes the Dirac equations for the spinor nucleon fields, nonhomogeneous Klein–Gordon equations for the meson fields, and an equation for the Coulomb field were obtained in [25–28] with the aid of Lagrange equations. The RMF models considered here disregard antiparticle states. We solved this set of coupled equations numerically by means of iterations. We attained good agreement for the single-particle spectra and bulk properties of nuclei with the results obtained by other authors and presented in the literature.

In order to perform calculations on the basis of the NRMF approach, we applied the Hartree–Fock method that was implemented with effective Skyrme nucleon–nucleon forces [29–31] and which is used most frequently to describe the structure of nuclei. For Skyrme forces, we choose the extended form [32–34]

$$V = t_0(1 + x_0P_\sigma)\delta(\mathbf{r}) + \frac{1}{2}t_1(1 + x_1P_\sigma) \quad (27)$$

$$\times \left[\mathbf{k}'^2\delta(\mathbf{r}) + \delta(\mathbf{r})\,\mathbf{k}^2\right] + t_2(1 + x_2P_\sigma)\,\mathbf{k}'\delta(\mathbf{r})\,\mathbf{k}$$
$$+ \frac{1}{6}t_3(1 + x_3P_\sigma)\,\rho^\gamma(\mathbf{R})\,\delta(\mathbf{r}) + \frac{1}{2}t_4(1 + x_4P_\sigma)$$
$$\times \left[\mathbf{k}'^2\rho^{\gamma_4}(\mathbf{R})\,\delta(\mathbf{r}) + \delta(\mathbf{r})\,\rho^{\gamma_4}(\mathbf{R})\,\mathbf{k}^2\right]$$
$$+ t_5(1 + x_5P_\sigma)\,\mathbf{k}'\rho^{\gamma_5}(\mathbf{R})\,\delta(\mathbf{r})\,\mathbf{k}$$
$$+ iW_0(\boldsymbol{\sigma}_1 + \boldsymbol{\sigma}_2)\left[\mathbf{k}' \times \delta(\mathbf{r})\,\mathbf{k}\right],$$

where we used the following generally adopted notation: $\mathbf{r} = \mathbf{r}_1 - \mathbf{r}_2$ and $\mathbf{R} = (\mathbf{r}_1 + \mathbf{r}_2)/2$ are, respectively, the relative radius vector and the radius vector of the center of mass of interacting nucleons; $\rho = \rho_n + \rho_p$, ρ_n, and ρ_p are, respectively, the total, neutron, and proton densities of the target nucleus; $\mathbf{k} = -i\partial/\partial\mathbf{r}$ and $\mathbf{k}' = i\partial/\partial\mathbf{r}'$ are the momentum operators for the relative motion of nucleons in, respectively, the initial and the final state; and P_σ is the spin-permutation operator. The nucleon–nucleon interaction being considered is characterized by the phenomenological parameters t_n, x_n $(n = 0–5)$, and W_0, which are determined, in just the same way as the parameters of the RMF model, from a fit to the properties of finite nuclei and infinite nuclear matter. The Hartree–Fock method with differently parametrized Skyrme forces was used by our group earlier [34, 35] in calculating the properties of various finite nuclei and infinite nuclear matter.

At the present time, many sets of parameters of RMF and NRMF models are available in the literature. We choose several parameter sets that were obtained by various authors in recent years and which were fitted to basic features of a large number of nuclei and to basic features of nuclear and neutron matter. All of the calculations on the basis of various mean-field models were performed with allowance for constraints adopted in the original studies of those authors—in particular, in the spin–orbit component of the Hartree–Fock Hamiltonian involving Skyrme interaction. In the calculations for the ^{40}Ca nucleus within all models where one does not include the correction for its center-of-mass motion, we took this motion into account, after obtaining a self-consistent solution, in the harmonic-oscillator approximation [36] by rescaling the neutron- and proton-density distributions according to the formulas

$$\rho_{\text{c.m.}}(r) \tag{28}$$
$$= \frac{1}{(2\pi)^3}\int d^3k \exp\left(i\mathbf{kr} + B^2k^2/4\right)\rho(k),$$
$$\rho(k) = \int d^3k \exp\left(-i\mathbf{kr}\right)\rho(r),$$

where $B^2 = \hbar/(\omega mA)$ and where we have used the well-known approximation $\hbar\omega = 41A^{-1/3}$ [MeV].

4. Employing the approach described above and based on the Glauber–Sitenko theory of multiple diffractive scattering with allowance for nucleon correlations, incorporated in our theoretical scheme via taking into account intermediate excitations of target nuclei, and with allowance for noneikonal corrections to proton–nucleus amplitudes, we have performed a series of calculations of differential cross sections and polarization observables for the elastic scattering of 800-MeV protons on ^{40}Ca and ^{208}Pb nuclei.

In just the same way as earlier in [8], the proton–nucleon amplitudes was replaced in our calculations by an approximation whose parameters were determined in [37] from the results of the partial-wave analysis performed in [12]. The form of this approximation and the values of its parameters at the energy of 800 MeV were presented in [8]. For the sake of comparison, the calculations based on different parametrizations known for the proton–nucleon amplitudes from the literature (for example, from [38]) and constructed by using the solutions of different partial-wave analyses were performed in our present study for some cases. The results of those calculations with different versions of the proton–nucleon amplitudes differ only slightly from one another.

In describing observables for the above cases of proton–nucleus scattering, we have performed a comparative analysis of the results obtained on the basis of a significant number of versions of calculations with nucleon densities found from microscopic calculations of the nuclear structure with various sets of parameters for the relativistic and nonrelativistic mean-field models of the nucleus, which were proposed in recent years by different authors. In the case of relativistic models, we have chosen the NL3* [26], FSUGold [27], FSUGZ03 [25] and IU-FSU [28] parameter sets. In the calculations with Skyrme nucleon–nucleon forces, we used both standard ($t_4 = t_5 = 0$) versions of these forces—TOV-min [39], SAMi [40], SLy5* [41], and UNEDF0 [42]—and their extended versions in (27) with allowance for terms involving the parameters t_4 and t_5, such as BSk18 [33], BSk20 [43], BSk24 [44], and SkOP4 [34]. The choice of these parameter versions was motivated by the fact that the respective values were determined on the basis of an analysis of basic features of a large number of nuclei, as well as the properties of nuclear and neutron matter. We also note that we found the SkOP4 forces from the conditions of optimization of a simultaneous description of nuclear-structure properties and observables of elastic nucleon–nucleus scattering within the microscopic optical model. For the sake of comparison, we additionally performed calculations with proton densities determined from model-independent charge distributions in the form of the sum of Gaussian functions (SOG) [45] by

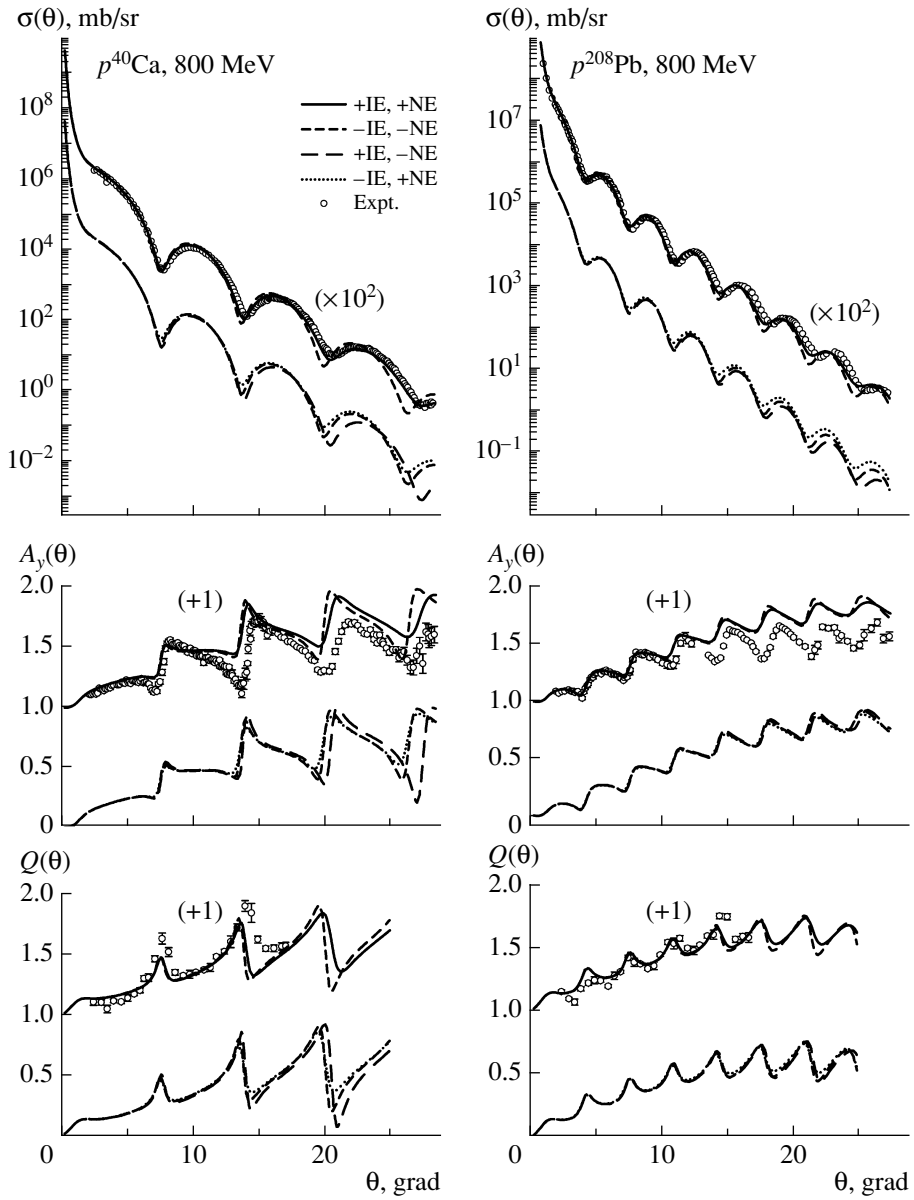

Fig. 1. Differential cross sections $\sigma(\theta)$, analyzing powers $A_y(\theta)$, and spin-rotation functions $Q(\theta)$ for elastic p^{40}Ca and p^{208}Pb scattering at 800 MeV according to calculations performed by using the SOG model-independent nucleon densities (+) with and (−) without allowance for intermediate excitations (IE) and noneikonal corrections (NE). The displayed experimental data were borrowed from [47–49].

eliminating the contribution of the proton charge form factor and with a similar model-independent neutron density for ^{208}Pb from [46] (for ^{40}Ca, we assumed that the model-independent neutron and proton densities are identical).

In calculating observables of proton–nucleus scattering, we took into account a number of corrections to the standard Glauber–Sitenko approach. In particular, we took into account nucleon correlations in just the same way as in [8] by including in our scheme several intermediate excitations (those whose quantum numbers are $I^\pi = 2^+, 3^-, 4^+$, and 5^-) both in the ^{40}Ca and in the ^{208}Pb nucleus, borrowing the values of their parameters from [8]. Also, we set the short-range correlation length to $l_{\rm cor} = 0.55$ fm.

Figure 1 gives the results that arise upon performing several versions of calculations of observables of p^{40}Ca and p^{208}Pb scattering and which demonstrate the effect of various included corrections. The observables in Fig. 1 were calculated by using the aforementioned model-independent nucleon densities. A comparison of the curves on display in Fig. 1 shows that the inclusion of two-nucleon correlations plays a significant role at not very small values of

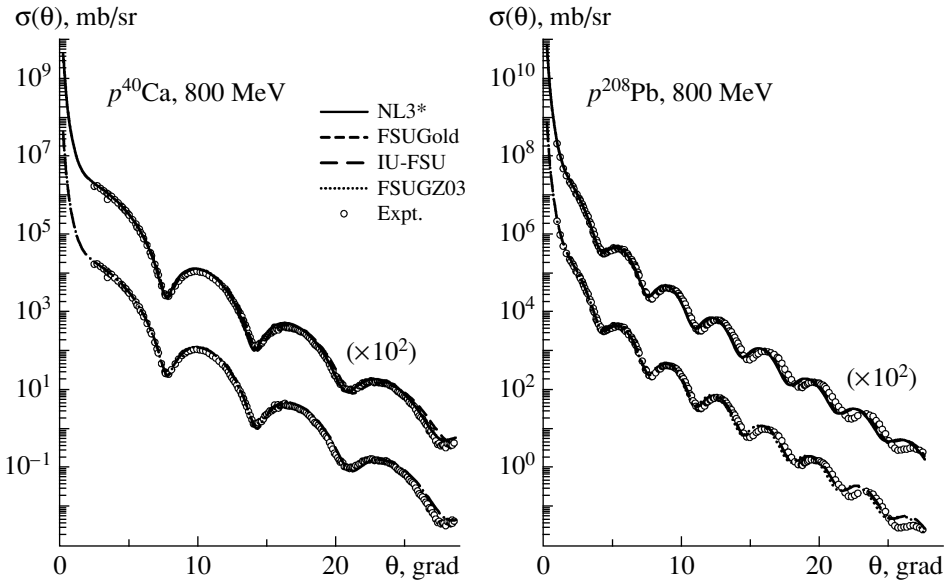

Fig. 2. Differential cross sections $\sigma(\theta)$ for elastic p^{40}Ca and p^{208}Pb scattering at 800 MeV according to calculations performed with the nucleon densities obtained in the RMF approximation with various parameter sets. The displayed experimental data were borrowed from [47, 48].

the scattering angle, as was also indicated in [8]. Their contribution leads to a shift of the positions of diffractive oscillations in the cross section and spin observable toward large scattering angles and enhances the rate of the decrease in the cross-section maxima as the scattering angle increases. Concurrently, the effect of noneikonal corrections becomes stronger. This effect manifests itself first of all in the filling of the minima of the differential cross sections and polarization observables. We note that the contribution of the noneikonal corrections to the cross section proves to be greater in the case of scattering on ^{208}Pb nuclei. We can conclude that the total contribution of the included corrections is quite significant at not very small scattering angles and that it leads to a substantial improvement of agreement between scattering cross sections calculated with model-independent nucleon densities and experimental data. The role of the corrections being considered appears to be similar in calculating observables by using different nucleon-density versions employed in the present study. In the following, we therefore present only the results of those calculations where we took into account all of the aforementioned corrections.

It is of interest to compare the results that we obtained by calculating observables of elastic proton–nucleus scattering on the basis of the theory of multiple diffractive scattering in the version considered here with the results of calculations that employ nucleon densities found by considering various versions of the description of the structure of nuclei both in the NRMF and in the RMF approximation. The results of this comparison are given below.

In Fig. 2, the differential cross sections for elastic p^{40}Ca and p^{208}Pb scattering at 800 MeV are given according to calculations with the nucleon densities obtained in the RMF approximation for the NL3*, FSUGold, FSUGZ03, and IU-FSU force versions. This figure shows that all of the RMF versions considered here yield rather close results. In the case of scattering on ^{40}Ca nuclei, all of these nucleon-density versions ensure good agreement between the calculated cross section and experimental data. Although the results of the calculations for scattering on ^{208}Pb nuclei are rather close to the experimental points in Fig. 2, a shift of cross-section oscillations toward smaller angles arises as the scattering angle grows.

The results of similar calculations of differential cross sections with nucleon densities obtained on the basis of the NRMF approximation with the TOV-min, SAMi, SLy5*, and UNEDF0 Skyrme forces of the standard form are given in Fig. 3, while the results for the BSk18, BSk20, BSk24, and SkOP4 extended Skyrme force versions are displayed in Fig. 4. In just the same way as in the calculations with the nucleon densities from the RMF models, the calculated cross sections in Figs. 3 and 4 are predominantly in fairly good agreement with the measured cross sections, even though there is a moderate shift of cross-section oscillations toward smaller angles; this is not so only in the case of the calculations with the SkOP4 forces. We note that the calculations with

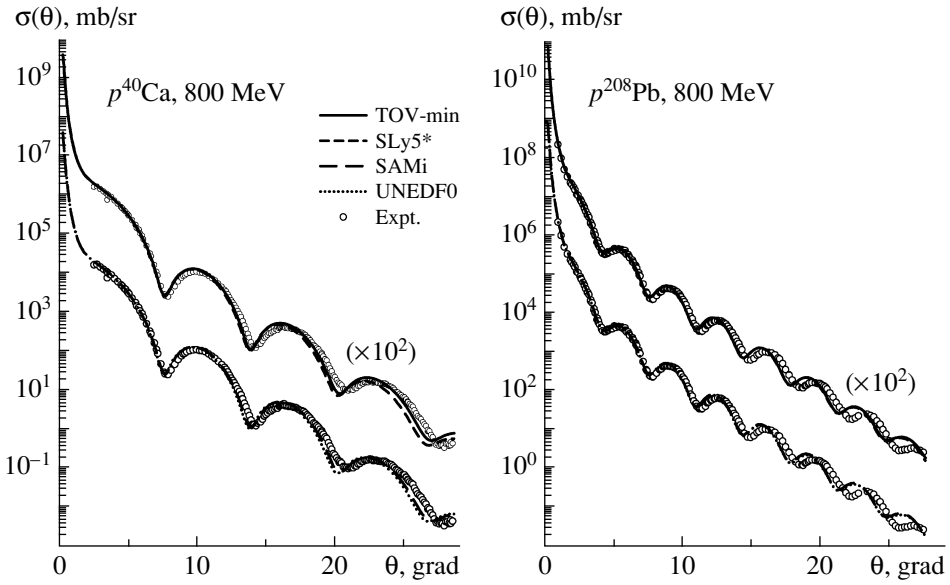

Fig. 3. As in Fig. 2, but for the calculations that employ the nucleon densities obtained in the NRMF approximation with the standard sets of parameters of Skyrme forces.

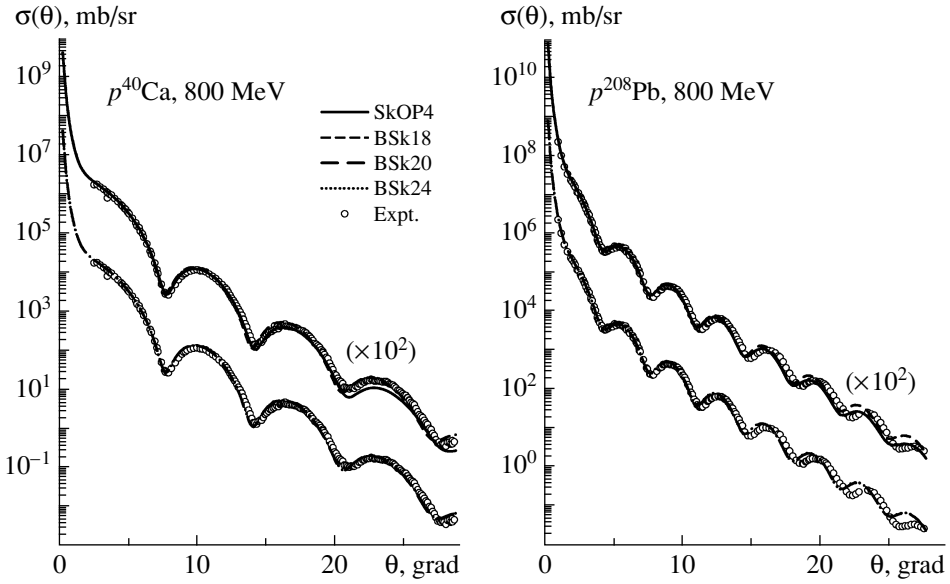

Fig. 4. As in Fig. 2, but for the calculations employing nucleon densities obtained in the NRMF approximation with various extended sets of parameters of Skyrme forces.

the SkOP4 extended Skyrme forces obtained in [34] provide a somewhat better description of the data on the angular distributions of the cross sections (especially for ^{208}Pb nuclei) than the calculations with the other Skyrme forces considered here. The possible reason is that the SkOP4 forces were obtained from an analysis of observables of elastic nucleon–nucleus scattering on the basis of the microscopic optical potential, which also depends substantially on the behavior of respective nucleon densities.

Figure 5 illustrates a comparison of the results obtained for the analyzing powers $A_y(\theta)$ and spin-rotation functions $Q(\theta)$ from calculations performed with various nucleon-density versions considered above. From Fig. 5, one can see that, by and large, the calculated polarization observables describe correctly the behavior of their measured counterparts. In the case of the analyzing power, however, theoretical curves obtained from all versions of the calculations, including calculations with model-independent

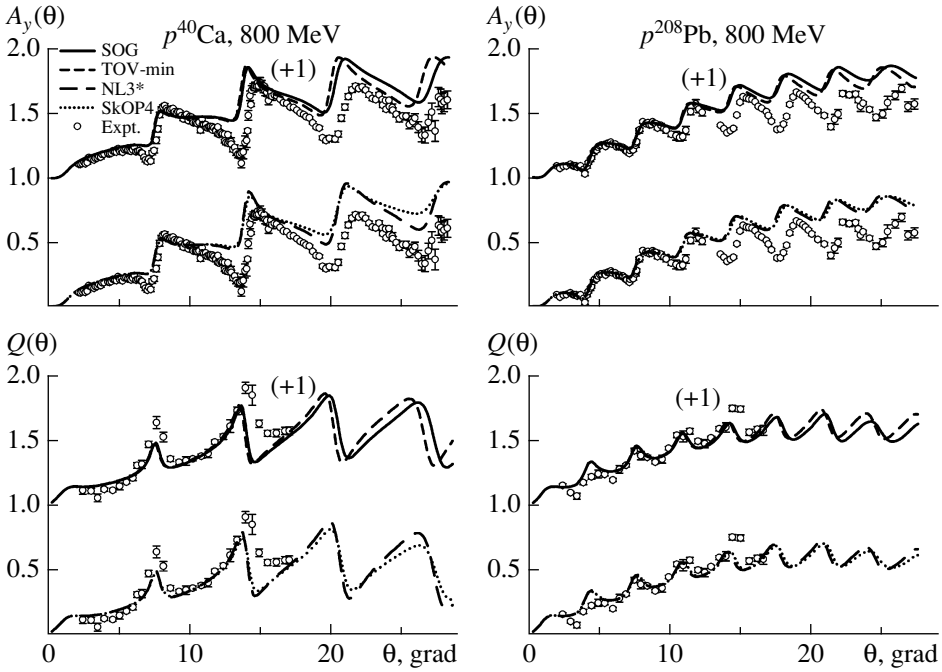

Fig. 5. Analyzing powers $A_y(\theta)$ and spin-rotation functions $Q(\theta)$ for elastic p^{40}Ca and p^{208}Pb scattering at 800 MeV according to calculations with various nucleon densities.

nucleon densities, go somewhat higher than the experimental points as the scattering angle grows. At the same time, the calculations provide a good description of available data for the spin-rotation function.

In the literature, there are presently some articles (see, for example, [50] and references therein) where data on proton–nucleus scattering in the energy region being considered are analyzed on the basis of the relativistic impulse approximation. In Fig. 6, we therefore present a comparison of the results of our calculations of observables for elastic p^{40}Ca scattering within the theory of multiple diffractive scattering with the results obtained in [50] on the basis of the relativistic impulse approximation. In these two versions of the calculations, use is made of the same nucleon densities calculated on the basis of the RMF model by using the NL3 parameter set [22]. Both the results of the calculations performed within the theory of multiparticle diffractive scattering and the results obtained on the basis of the RMF model agree well with experimental data. Specifically, the theory of multiple diffractive scattering provides a better description of the differential cross section, while the calculations in the relativistic impulse approximation yield better results for the analyzing power. The two approaches in question yield very close results for the spin-rotation function. It should also be noted that model-independent nucleon densities, which were used here in the calculations whose results are shown in Fig. 1, were applied in [46] in calculating observables in the relativistic impulse approximation for elastic p^{208}Pb scattering at 295 MeV.

5. In the present study, we have performed a comparative analysis of employing different versions of the proton and neutron densities in target nuclei in the calculations of the differential cross sections and spin observables for elastic p^{40}Ca and p^{208}Pb scattering at the energy of 800 MeV on the basis of the Glauber–Sitenko theory of multiple diffractive scattering. In doing this, we have considered nucleon densities calculated on the basis of models used presently to describe the structure of nuclei in the relativistic- and nonrelativistic-mean-field approximations, as well as model-independent densities from the literature. In our calculations on the basis of the theory of multiple diffractive scattering, we have employed expressions that we proposed earlier for the amplitudes for elastic proton–nucleus scattering and which take into account distinctions between proton–proton and proton–neutron amplitudes and between the neutron and proton densities, Z ordering of spin operators, electromagnetic effects, and the effect of two-nucleon correlations included via taking into account intermediate excitations of target nuclei. This approach was extended via the inclusion of noneikonal corrections that arise in the proton–nucleus amplitudes calculated within the theory of multiple diffractive scattering because of the possible deviations of the incident proton from the eikonal

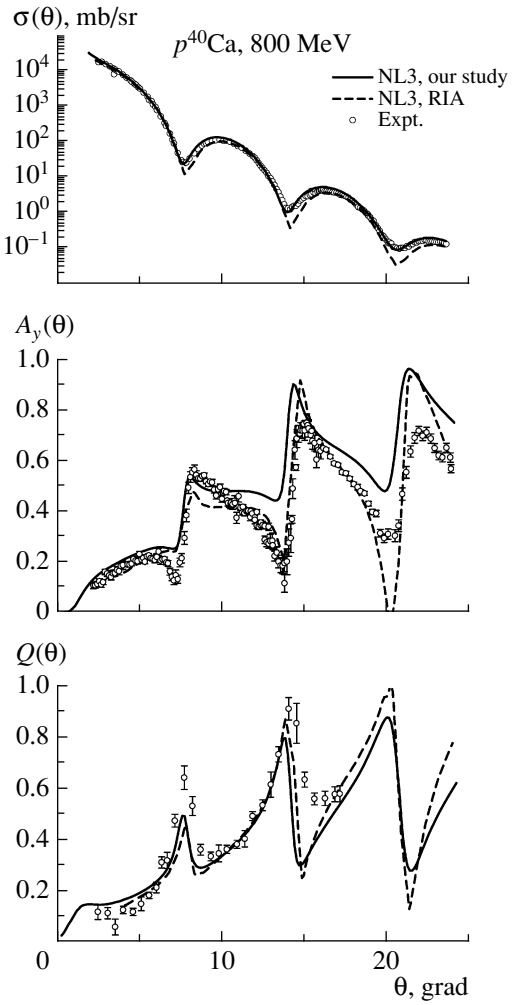

Fig. 6. Differential cross sections $\sigma(\theta)$, analyzing powers $A_y(\theta)$, and spin-rotation functions $Q(\theta)$ for elastic p^{40}Ca scattering at 800 MeV according to calculations with the nucleon densities based on the RMF model with the NL3 parameter set in the theory of multiple diffractive scattering (solid curve) and on the relativistic impulse approximation (RIA) (from [50]—dashed curve).

propagation between successive events of interaction with target nucleons.

We have studied the effect of simultaneously taking into account noneikonal corrections to the theory of multiple diffractive scattering and two-nucleon correlations on the description of cross sections and spin observables. The contribution of intermediate excitations of target nuclei is of importance in the calculations being considered. This contribution leads to a shift of positions of diffraction oscillations toward large scattering angles and reduces cross-section maxima, this effect becoming more pronounced as the scattering angle increases. The inclusion of noneikonal corrections manifests itself in reducing the depth of diffraction minima (smoothing them) of observables. The relative magnitude of this effect depends on the target nucleus. The total contribution of the corrections included here is significant at not very small values of the scattering angle and improves agreement with experimental data; therefore, we took it into account in a comparative analysis of calculations with different nuclear densities.

Our calculations revealed that the majority of nucleon densities used in the present study and obtained for modern versions of nucleon interaction in the relativistic- and nonrelativistic-mean-field approximations provide a nearly identical description of observables of elastic proton–nucleus scattering on the basis of the theory of multiple diffractive scattering in the version that we consider here and which includes the aforementioned corrections. This description is in fairly good agreement with experimental data. We note, however, that, in all of the calculations performed here for the analyzing power, the calculated curve goes somewhat higher as the scattering angle grows than the experimental points, especially in the case of scattering on ^{208}Pb nuclei. This is likely to be indicative of flaws inherent in the model used. It can be assumed that a more consistent relativistic description of the process of multiple incident-proton scattering on target nucleons is required for further refinements upon the model.

The best description of observables is ensured by the use of model-independent nucleon densities found in the literature from an analysis of scattering processes. We also emphasize that the nucleon densities for the SkOP4 Skyrme forces that we found from an analysis of nucleon–nucleus scattering on the basis of the microscopic optical potential also lead to fairly good agreement with data.

REFERENCES

1. R. J. Glauber, in *Lectures in Theoretical Physics*, Ed. by W. E. Brittin and L. G. Dunham (Interscience, New York, 1959), Vol. 1, p. 315.
2. A. G. Sitenko, Ukr. Fiz. Zh. **4**, 152 (1959).
3. A. G. Sitenko, *Theory of Nuclear Reactions* (World Scientific, Singapore, 1990).
4. L. Ray, G. W. Hoffmann, and W. R. Coker, Phys. Rep. **212**, 223 (1992).
5. B. C. Clark, L. J. Kerr, and S. Hama, Phys. Rev. C **67**, 054605 (2003).
6. Ch. Elster et al., Phys. Rev. C **78**, 034002 (2008).
7. M. N. Platonova and V. I. Kukulin, Phys. Rev. C **81**, 014004 (2010).
8. V. I. Kuprikov and V. V. Pilipenko, Phys. At. Nucl. **63**, 782 (2000).
9. V. V. Pilipenko and V. I. Kuprikov, Ukr. J. Phys. **48**, 1024 (2003).
10. P. Osland and R. J. Glauber, Nucl. Phys. A **326**, 255 (1979).

11. G. D. Alkhazov, S. I. Belostocky, and A. A. Vorobyov, Phys. Rep. **42**, 89 (1978).
12. J. Bystricky et al., J. Phys. (Paris) **48**, 199 (1987).
13. S. Raman et al., At. Data Nucl. Data Tables **36**, 1 (1987).
14. R. H. Spear, At. Data Nucl. Data Tables **42**, 55 (1989).
15. S. J. Wallace, Phys. Rev. C **12**, 179 (1975).
16. M. Bleszynski and P. Osland, Phys. Lett. B **84**, 157 (1979).
17. M. L. Goldberger and K. M. Watson, *Collision Theory* (Wiley, New York, 1967).
18. I. Ahmad, Nucl. Phys. A **247**, 418 (1975).
19. J. D. Walecka, Ann. Phys. (N. Y.) **83**, 491 (1974).
20. C. Horowitz and B. D. Serot, Nucl. Phys. A **368**, 503 (1981).
21. Y. K. Gambhir, P. Ring, and A. Thimet, Ann. Phys. (N. Y.) **198**, 132 (1990).
22. G. A. Lalazissis, J. König, and P. Ring, Phys. Rev. C **55**, 540 (1997).
23. R. Furnstahl, B. D. Serot, and H.-B. Tang, Nucl. Phys. A **615**, 441 (1997).
24. B. D. Serot and J. D. Walecka, Int. J. Mod. Phys. E **6**, 515 (1997).
25. R. Kumar, B. K. Agrawal, and S. K. Dhiman, Phys. Rev. C **74**, 034323 (2006).
26. G. A. Lalazissis et al., Phys. Lett. B **671**, 36 (2009).
27. B. G. Todd-Rutel and J. Piekarewicz, Phys. Rev. Lett. **95**, 122501 (2005).
28. F. J. Fattoyev et al., Phys. Rev. C **82**, 055803 (2010).
29. T. H. R. Skyrme, Nucl. Phys. **9**, 615 (1958–1959).
30. D. Vautherin and D. M. Brink, Phys. Rev. C **5**, 626 (1972).
31. J. R. Stone and P.-G. Reinhard, Prog. Part. Nucl. Phys. **58**, 587 (2007).
32. S. Krewald et al., Nucl. Phys. A **281**, 166 (1977).
33. N. Chamel, S. Goriely, and J. M. Pearson, Phys. Rev. C **80**, 065804 (2009).
34. V. V. Pilipenko and V. I. Kuprikov, Phys. Rev. C **86**, 064613 (2012).
35. V. Yu. Gonchar, E. V. Inopin, and V. I. Kuprikov, Sov. J. Nucl. Phys. **25**, 25 (1977).
36. J. W. Negele, Phys. Rev. C **1**, 1260 (1970).
37. I. N. Kudryavtsev and A. P. Soznik, J. Phys. G **15**, 1377 (1989).
38. J. A. McNeil, L. Ray, and S. J. Wallace, Phys. Rev. C **27**, 2123 (1983).
39. J. Erler et al., Phys. Rev. C **87**, 044320 (2013).
40. X. Roca-Maza, G. Colò, and H. Sagawa, Phys. Rev. C **86**, 031306(R) (2012).
41. A. Pastore et al., Phys. Scr. T **154**, 014014 (2013).
42. M. Kortelainen et al., Phys. Rev. C **85**, 024304 (2012).
43. S. Goriely, N. Chamel, and J. M. Pearson, Phys. Rev. C **82**, 035804 (2010).
44. S. Goriely, N. Chamel, and J. M. Pearson, Phys. Rev. C **88**, 024308 (2013).
45. H. de Vries, C. D. Jager, and C. de Vries, At. Data Nucl. Data Tables **36**, 495 (1987).
46. J. Zenihiro et al., Phys. Rev. C **82**, 044611 (2010).
47. E. Bleszynski et al., Phys. Rev. C **25**, 2563 (1982).
48. G. W. Hoffmann et al., Phys. Rev. C **21**, 1488 (1980).
49. R. W. Fergerson et al., Phys. Rev. C **33**, 239 (1986).
50. M. Bhuyan et al., Phys. Rev. C **82**, 064602 (2010).